

# A MULTISCALE METHOD FOR MODELING TRANSPORT IN POROUS MEDIA ON UNSTRUCTURED CORNER-POINT GRIDS

JØRG E. AARNES AND YALCHIN EFENDIEV

**ABSTRACT.** Multiscale solution methods are currently under active investigation for the simulation of subsurface flow in heterogeneous formations. These procedures capture the effects of fine-scale permeability variations through the calculation of specialized coarse-scale basis functions. Most of the multiscale techniques presented to date address subgrid capturing in pressure solution (elliptic/parabolic equations). In this paper we propose a multiscale method for solving transport equations on a coarse grid. In this method the global flow is computed on a coarse grid scale, but information from a fine scale velocity field is used to improve accuracy. The method is applied to incompressible and immiscible two-phase flow on a synthetic geological model with corner-point grid geometry. Although corner-point grids are given on a logically Cartesian format, the resulting grids are unstructured in physical space. The numerical results demonstrate that the multiscale method gives nearly the same flow characteristics as simulations where the transport equation is solved on the scale of an underlying fine grid.

## 1. INTRODUCTION

Subsurface formations typically exhibit heterogeneities spanning a wide range of length scales. Through the use of sophisticated geological and geostatistical modeling tools, engineers and geologists can now generate highly detailed, three dimensional representations of reservoir properties. Such models can be particularly important for reservoir management, as fine scale details in formation properties, such as thin high permeability layers or thin shale barriers, can dominate reservoir flow behavior. The direct use of these highly resolved models for reservoir simulation is not generally feasible because their fine level of detail (tens of millions of cells or grid blocks) places prohibitive demands on computational resources. Typically, upscaled or multiscale models are employed for such systems. The main idea of upscaling techniques is to form coarse-scale equations with a prescribed analytical form that may differ from the underlying fine-scale equations. In multiscale methods, the fine-scale information is carried throughout the simulation and the coarse-scale equations are generally not expressed analytically, but rather formed and solved numerically.

Most of the multiscale techniques presented to date address subgrid capturing in the pressure solution which has an elliptic nature. In this paper we propose a multiscale method for solving transport equations for the saturation field. More difficulties are typically encountered in developing multiscale methods for the saturation equation. Due to the hyperbolic nature of this equation, and the high correlation length features often present in the fine scale permeability field, distant (nonlocal) effects can strongly impact coarse grid parameters. This renders coarse grid properties dependent on global boundary conditions and can lead to process dependence (i.e., a lack of robustness) in the coarse grid description. Our approach entails the computation of the saturation on a coarse grid scale using the information from a fine scale velocity field.

---

*Key words and phrases.* multiscale methods, porous media, two-phase flow, upscaling.

The research of J. E. Aarnes was partially supported by Shell and the Research Council of Norway under grants 158908/420 and 175962/S30. The research of Y. Efendiev was partially supported by NSF grants DMS-0327713 and EIA-0540138 and DOE grant DE-FG02-05ER25669.

The method is based on a finite volume methodology that resolves both coarse scale and fine scale flow patterns. The proposed method is suitable for complex unstructured grids, including general corner-point grids, the industry standard in reservoir modeling and simulation and has some similarities with the multiscale framework developed for nonlinear equations [12], and with pseudo type approaches [15, 8, 16], but there are also important differences. The basic idea behind the current method is to solve first the global flow on a coarse grid, and then to recover a plausible saturation field on an underlying fine grid from the coarse scale solution. The main task in this approach is to determine the map from a coarse grid to a finer subgrid that reflects important fine scale features in the velocity field, and accounts for flow history. Once this map is determined, the proposed coarse grid formulation allows to compute the saturation field on the coarse grid.

The proposed methodology is based on a sequential splitting of the governing equations into an elliptic equation for pressure and velocities, and a hyperbolic (or parabolic) equation that models the phase transport. The elliptic part is solved on a coarse grid with a multiscale mixed finite element method [5, 3]. This method provides high resolution velocity fields at low computational cost. Multiscale finite element methods, as proposed in [13], and their modifications are not new in porous media flow simulations. In previous findings, multiscale finite element methodology has been modified and successfully applied to two-phase flow simulations in [14] and in [9, 5]. Arbogast ([6]) used variational multiscale strategy for capturing the subgrid effects in two-phase flow simulations. We remark that special basis functions in finite element methods have been used earlier in [7].

The paper is organized as follows. In Section 2 we introduce the equations for immiscible and incompressible two-phase flow. In Section 3 we present the multiscale mixed finite element method (MsMFEM) [3] that is used to compute flow velocities. In Section 4 we describe the new multiscale method for solving the transport equation and provide the analysis of the proposed method. Finally, numerical results are presented in Section 5 to demonstrate the performance of the methodology on a corner-point grid model.

## 2. MATHEMATICAL MODEL

We consider immiscible and incompressible two-phase flow without effects from gravity and capillary pressure. The equations are derived from conservation of mass for each phase  $j$ :

$$\phi \frac{\partial S_j}{\partial t} + \nabla \cdot v_j = q_j,$$

where the phase velocities  $v_j$  are given by Darcy's law:

$$v_j = -\lambda_j K \nabla p_j.$$

Here  $\phi$  is the porosity,  $S_j$  is the  $j$ -phase saturation (fraction of the void occupied by phase  $j$ ) and  $q_j$  is a source (or sink) term. In Darcy's law,  $K$  is the permeability tensor,  $p_j$  is the phase pressure and,  $\lambda_j = k_{rj}/\mu_j$ , where  $k_{rj}$  and  $\mu_j$  are the relative permeability and viscosity of phase  $j$  respectively. The relative permeability models the reduced conductivity of a phase due to the presence of other phases, and is assumed to be function of the saturations only.

Let the two phases be oil and water ( $j = o, w$ ). Since we neglect effects from capillary pressure so that  $\nabla p_o = \nabla p_w$ , we assume  $p_o = p_w = p$ . Then the Darcy equations combined with conservation of mass yields the *pressure equation*:

$$\begin{aligned} v &= -\lambda(S_w, S_o) K \nabla p, \\ \nabla \cdot v &= q, \end{aligned} \tag{1}$$

where  $v = v_w + v_o$ ,  $\lambda = \lambda_w + \lambda_o$ , and  $q = q_w + q_o$ .

If we assume that the two phases occupy the void space completely, i.e., that  $S_w + S_o = 1$ , and introduce the water *fractional flow*  $f_w(S_w) = \lambda_w(S_w)/\lambda(S_w, 1 - S_w)$ , then we may write the conservation equation for water, henceforth called the *saturation equation*, as follows:

$$\phi \frac{\partial S_w}{\partial t} + \nabla \cdot (f_w v) = q_w. \quad (2)$$

The system of equations (1)–(2) will be solved using a sequential splitting, i.e., the pressure equation is solved at the current time-step using saturation values from the previous time-step. Moreover, for ease of notation, we will henceforth drop the  $w$ -subscripts of  $S_w$ .

### 3. A MULTISCALE MIXED FINITE ELEMENT METHOD FOR ELLIPTIC PROBLEMS

Let  $\Omega \subset \mathcal{R}^d$ , and denote by  $n$  the outward pointing unit normal on  $\partial\Omega$ . In mixed formulations of (1) with no-flow boundary conditions on  $\partial\Omega$ , one seeks  $(v, p) \in H_0^{\text{div}}(\Omega) \times L^2(\Omega)$  such that

$$\int_{\Omega} v \cdot (\lambda K)^{-1} u \, dx - \int_{\Omega} p \nabla \cdot u \, dx = 0 \quad \text{for all } u \in H_0^{\text{div}}(\Omega), \quad (3)$$

$$\int_{\Omega} l \nabla \cdot v \, dx = \int_{\Omega} ql \, dx \quad \text{for all } l \in L^2(\Omega). \quad (4)$$

Here  $H_0^{\text{div}}(\Omega) = \{v \in (L^2(\Omega))^d : \nabla \cdot v \in L^2(\Omega) \text{ and } v \cdot n = 0 \text{ on } \partial\Omega\}$ . Note that to determine  $p$  one must add an additional constraint such as  $\int_{\Omega} p = 0$ .

In a mixed FEM discretization of (3)–(4), the spaces  $H_0^{\text{div}}(\Omega)$  and  $L^2(\Omega)$  in which we seek the pressure and velocity solutions are replaced by finite dimensional subspaces, say  $U$  and  $V$ , that typically consists of low order piecewise polynomials. In a MsMFEM one attempts to design the approximation space for velocity in such a way that it embodies the impact of subgrid variations in  $K$ . The MsMFEM outlined below [3] is a variant of the method introduced by Chen and Hou [9] that, in addition to giving mass conservative velocity fields on the discretization grid (the coarse grid), provides a mass conservative velocity field on an underlying subgrid. This feature allows users to choose grids for flow and transport simulations in a nearly seamless fashion.

To formulate the MsMFEM introduced in [3], let  $\mathcal{T} = \{T_i\}$  be a grid where each grid block  $T$  is a connected union of grid cells in an underlying subgrid  $\mathcal{K} = \{K_i\}$ . The grid  $\mathcal{T}$  will be referred to as the *coarse grid*, and the subgrid  $\mathcal{K}$  will be referred to as the *fine grid*. Let the approximation space for pressure be the space of piecewise constant functions on  $\mathcal{T}$ , i.e.,

$$U = \text{span}\{u \in L^2(\Omega) : u|_T \text{ is constant for all } T \in \mathcal{T}\}.$$

To define the approximation space  $V$  for velocity  $v$ , denote by  $\Gamma_{ij} = \partial T_i \cap \partial T_j$  the non-degenerate interfaces in the coarse grid. To each interface, we assign a corresponding basis function  $\psi_{ij}$ . This basis function is supported in  $\Omega_{ij} = T_i \cup \Gamma_{ij} \cup T_j$ , and is related to a function  $\phi_{ij}$  through Darcy's law:  $\psi_{ij} = -\lambda K \nabla \phi_{ij}$ . The function  $\phi_{ij}$ , and thus also the basis function  $\psi_{ij}$ , is obtained by solving (numerically) the following local elliptic problem:

$$\psi_{ij} \cdot n_{ij} = 0 \text{ on } \partial\Omega_{ij}, \quad \nabla \cdot \psi_{ij} = \begin{cases} f_i(x)/\int_{T_i} f_i(x)dx & \text{for } x \in T_i, \\ -f_j(x)/\int_{T_j} f_j(x)dx & \text{for } x \in T_j. \end{cases} \quad (5)$$

Here  $n_{ij}$  is the outward pointing unit normal on  $\partial\Omega_{ij}$ , and

$$f_i = \begin{cases} f & \text{if } \int_{T_i} f \, dx \neq 0, \\ \lambda \text{trace}(K) & \text{else.} \end{cases} \quad (6)$$

The MsMFEM approximation space  $V$  for velocity is now the span of the basis functions  $\{\psi_{ij}\}$ .

The source terms  $\{f_i\}$  are chosen as defined by (6) for the following reasons. First, they produce basis functions that force unit flux across associated coarse grid interfaces, i.e.,  $\int_{\Gamma_{ij}} \psi_{ij} \cdot n_{ij} = 0$ .

$n ds = 1$ , where  $n$  is the unit normal to  $\Gamma_{ij}$  pointing into  $T_j$ . This implies that the MsMFEM solution  $\{v_{ij}\}$  for velocity gives the fluxes across the respective coarse grid interfaces. Second, if a conservative method is used to compute basis functions, then the velocity  $v = \sum v_{ij} \psi_{ij}$  conserves mass on the subgrid  $\mathcal{K}$ . Third, choosing special source terms in blocks with a source allows the method to model radial flow around point or line sources, such as wells in oil-reservoirs, on the subgrid scale. Finally, by letting  $f_i$  scale according to the permeability as in (6), one can to some extent avoid unnaturally high flow velocities in low-permeable fine grid cells.

The computational complexity of a MsMFEM is not significantly less than the computational complexity of solving the full problem on the fine grid with a (very) efficient linear solver. Note, however, that the most expensive task in a MsMFEM, the computation of the basis functions is perfectly parallel computation since each basis function  $\psi_{ij}$  can be computed independently. Another advantage for the purpose of running two-phase flow simulations, for which the pressure equation (1) needs to be solved multiple times due to dynamic changes in the mobility  $\lambda$ , is that basis functions often need to be recomputed only when flow conditions change significantly. This claim is supported by an analysis of the saturation dependence in the pressure solution [11]. Here it is shown that when flow conditions do not change, the time varying velocity field is strongly influenced by the initial velocity field. The computation of basis functions then becomes part of a preprocessing step, and MsMFEMs become analogous to single-phase flow upscaling methods, see e.g., [10] and references therein. The computational complexity of a MsMFEM is also comparable to the computation cost of single-phase flow upscaling procedures. We should add, however, that numerical experiments show that if saturation profiles exhibit sharp fronts, then a slight improvement in accuracy can be obtained by regenerating basis functions in regions where the saturation has changed substantially since the previous time-step [5]. Similar observations was made by Jenny et al. [14] for the multiscale finite volume method.

#### 4. A MULTISCALE METHOD FOR HYPERBOLIC TRANSPORT EQUATIONS

The key idea behind the multiscale method that we propose here is to use information from a velocity field with subgrid resolution to improve accuracy of flow simulations on coarse grids. To give an outline of the algorithm, denote, as in Section 3, the coarse grid by  $\mathcal{T} = \{T_i\}$  and an underlying fine grid by  $\mathcal{K} = \{K_i\}$ . Although we employ the same notation as in Section 3, the grids used here need not coincide with the coarse and fine grids for the MsMFEM. However, we assume that the MsMFEM provides fluxes across all fine grid interfaces  $\{\gamma_{kl} = \partial K_k \cap \partial K_l\}$ .

The basic algorithm for the proposed multiscale method reads as follows:

For each  $T_i \in \mathcal{T}$ , compute

$$\bar{S}_i^{n+1} = \bar{S}_i^n + \frac{\Delta t}{\int_{T_i} \phi dx} \left[ \int_{T_i} q_w(S^n) dx - \sum_{\gamma_{kl} \subset \partial T_i} V_{kl}(S^n) \right], \quad (7)$$

and set  $S^{n+1}|_{T_i} = I_{T_i}(\bar{S}_i^{n+1})$ .

Here  $\Delta t$  denotes the time-step,  $\bar{S}_i^n$  the net saturation in  $T$  at time  $t = t_n$ , and

$$V_{kl}(S) = \max\{v_{kl} f_w(S_i), -v_{kl} f_w(S_j)\},$$

where  $v_{kl}$  is the Darcy flux across the corresponding *fine grid* interface  $\gamma_{kl}$  that we get from the MsMFEM. Thus,  $V_{kl}$  is the standard upstream flux function with respect to  $\gamma_{kl}$ . The operators  $\{I_T : T \in \mathcal{T}\}$  map each grid block saturation onto plausible fine grid saturation fields inside the respective blocks. Thus, for each time-step, we update first coarse grid-block saturation values, and then map the coarse grid saturation field onto a plausible fine-grid saturation field.

Observe that in (7) the flux across  $\partial T$  is evaluated by summing fluxes across the fine grid interfaces  $\gamma_{kl} \subset \partial T$ . Thus, rather than using flux functions that model the total flux across coarse grid interfaces as functions of the net saturation in the upstream block, we evaluate the term  $f_{wv}$  in (2) on the scale of the fine grid. This requires that we have fine grid saturation values in all cells adjacent to grid block boundaries. The coarse-to-fine grid interpolation operators  $\{I_T\}$  are therefore not just tools to get better resolution, they also help to improve global accuracy of the multiscale method by providing a better approximation to flow across coarse grid interfaces. Indeed, without the interpolation operators, the flow across the coarse grid interfaces would have to be computed on the basis of the net grid block saturations only. This will cause loss of accuracy unless proper pseudo-functions [15, 16, 8] are used.

**4.1. The coarse-to-fine grid interpolation operators.** In the following we attempt to construct operators that map each coarse grid saturation field onto a fine scale saturation profile that is close to the corresponding profile that one would get by solving saturation equation on the global fine grid. The basic idea is to approximate the fine grid saturation in  $T_i$  as a linear combination two basis functions  $\Phi_i^k$  and  $\Phi_i^{k+1}$  with  $\int_{T_i} \Phi_i^k \phi dx \leq \bar{S}_i^n \int_{T_i} \phi dx < \int_{T_i} \Phi_i^{k+1} \phi dx$ :

$$I_{T_i}(\bar{S}_i^n) = \omega \Phi_i^k + (1 - \omega) \Phi_i^{k+1}. \quad (8)$$

The basis functions  $\Phi_i^k = \chi_i(x, \tau_k)$  represent snapshots of the solution of the following equation:

$$\phi \frac{\partial \chi_i}{\partial t} + \nabla \cdot (f_w(\chi_i)v) = q_w \quad \text{in } T_i. \quad (9)$$

That is, each basis function is the solution of the local problem (9) at a particular time instant  $\tau_k$ . Note that  $\tau$  here refers to time for the temporal evolution of  $\chi_i$ , and not related to the time  $t$  for the temporal evolution of the global solution  $S$ , i.e.,  $k$  is not related to  $n$ .

The parameter  $\omega$  in the interpolation (8) is chosen such that the interpolation preserves mass, i.e., such that

$$\int_{T_i} I_{T_i}(\bar{S}_i^n) \phi dx = \bar{S}_i^n \int_{T_i} \phi dx.$$

To minimize the interpolation error it is important that the basis functions span the range of saturation values with nearly equidistant interpolation points, i.e., the values

$$\frac{1}{\int_{T_i} \phi dx} \int_{T_i} \Phi_i^k \phi dx$$

should be approximately uniformly distributed in the interval  $[0, 1]$ . The “snapshots” that define the multiscale basis functions are therefore selected to satisfy this criteria.

Finally, for the local problem (9) to be well-defined, we need to specify initial conditions and boundary conditions, and provide a possibly time-varying velocity field in  $T_i$ . We assume below that the local equations (9) are solved using an upstream-weighted finite volume method. Thus, we need only specify boundary conditions on the inflow boundaries  $\Gamma_T^{\text{in}} = \{\gamma_{jl} \subset \partial T : K_l \subset T, v_{jl} < 0\}$ .

Conceptually it is possible to reconstruct a fine grid saturation profile provided that we know what the velocity field will be during the simulation, and know the correct initial and boundary conditions. However, we do not know *a priori* what the velocity will be, nor what boundary conditions to impose. Assumptions must therefore be made to approximate how the velocity and saturation evolve.

We describe first a *local approach* that was introduced in [1] in which no knowledge of what happens in “real-time” is required. This approach assumes that global boundary conditions for the pressure equation (1) are not changed, and that the source term  $q$  is fixed. Hence, in this

approach we assume that the velocity changes only due to variations in the total mobility  $\lambda$ . This implies that flow patterns will generally not change significantly from one time step to the next. One can therefore use the velocity field  $v$  obtained by solving the pressure equation (1) at initial time to estimate how the saturation profile will evolve locally. In the multiscale formulation introduced in [1] we construct the saturation basis functions (9) using  $v = v(x, t_0)|_T$  and  $f_w = 1$  on  $\Gamma_T^{\text{in}}$ .

Next, we introduce a new *global approach* that is capable of accounting for significant changes in flow conditions during simulation. To this end we need to build more information about the global problem into the local equations. In particular, in order to allow the velocity  $v$  in (9) to be updated whenever global flow conditions change, the time-scale in the local problems has to be the same as for the global problem (2). One option is to solve the local problems “simultaneously”, and use solutions in neighboring grid-blocks at the previous time-step to impose boundary conditions. Thus, in this approach the basis functions  $\Phi_i^k$  are sampled locally from solutions obtained using the following domain decomposition algorithm:

For each  $T \in \mathcal{T}$ , do

$$S_i^{n+1} = S_i^n + \frac{\Delta t}{\int_{K_i} \phi \, dx} \left[ \int_{K_i} q_w(S^{n+1}) \, dx - \sum_{j \neq i} V_{ij}^* \right] \quad \forall K_i \subset T, \quad (10)$$

where

$$V_{ij}^* = \begin{cases} V_{ij}(S^n) & \text{if } \gamma_{ij} \subset \Gamma_T^{\text{in}}(t_n), \\ V_{ij}(S^{n+1}) & \text{otherwise.} \end{cases}$$

Although the global approach is not significantly less computational expensive than a full simulation on the fine grid, there are reasons why this approach could still be justified. Clearly, the domain decomposition method (DDM) is easily parallelizable, and have reduced memory requirements. This can help accelerate simulations, and solve very large problems, also on single-processor computers. However, a drawback with the DDM is that it gives mass balance errors. By using the multiscale algorithm with interpolation operators generated using the DDM, one eliminates mass balance errors while preserving the main flow trends on the fine grid. The multiscale algorithm with basis functions generated using the DDM can therefore be viewed as a way of correcting solutions obtained with the DDM for mass balance errors.

For applications to reservoir simulation, there are other important reasons why the global approach may be preferred to the local approach. First, flow conditions in real reservoirs change frequently due to frequent changes in well-rates and well configurations. The cost of regenerating the local saturation basis functions each time flow conditions change could therefore easily exceed the cost of running a full simulation with the DDM. Second, to account for uncertainty in geostatistical reservoir models, it is common to run simulations on multiple realizations of the reservoir. These simulations are performed with the same injection-production history, only the geostatistics are changed. Hence, if the permeability changes in a way that does not alter flow patterns significantly, then saturation basis functions obtained for one realization could be used to run coarse grid simulations on other realizations at low computational cost. Finally, the computational cost of the multiscale algorithms can be efficiently reduced if it is combined with an adaptive strategy that uses multiscale basis functions only where fine grid information is important. This issue was explored for the local approach in [1].

**4.2. Analysis.** Next, we present the analysis of the proposed approach. The analysis is based on some of the estimates derived in [1]. The first step of the analysis is to separate the error that stems from the coarse grid equation (7) from the error that stems from the interpolation

of the coarse-grid saturation field onto a fine-grid saturation field. Denote

$$\bar{S}^n = \frac{1}{|T|} \int_T S^n dx,$$

where  $S^n = S(x, t_n)$  is the fine scale saturation field at time  $t = t_n$ , and denote by  $\bar{S}_h^n$  the corresponding saturation field obtained using the proposed multiscale technique. In the rest of the analysis, we will assume that the velocity field used in (9) is exact, i.e. that  $v = v(x, S(x, t_0))$  at all times  $t > 0$ , and neglect the source terms.

We will present the analysis for a generic coarse grid block, and thus ignore the index of a coarse grid block. Denote

$$F(S) = -\frac{1}{\int_T \phi(x) dx} \int_{\partial T} f_w(S)(v \cdot n) ds.$$

Then (7) in each  $T$  can be written as

$$\bar{S}_h^{n+1} = \bar{S}_h^n + \Delta t F(I(\bar{S}_h^n)) + o(\Delta t). \quad (11)$$

For simplicity, the remainder is denoted by  $o(\Delta t)$ . Note that this error is due to temporal (backward Euler) discretization. If the average saturation is a smooth function with respect to time then the remainder is  $O((\Delta t)^2)$ .

The equation for average of fine-scale saturation can be obtained by averaging the fine-scale equation:

$$\bar{S}^{n+1} = \bar{S}^n + \Delta t F(S^n) + o(\Delta t). \quad (12)$$

Our objective is to estimate the error  $\delta^{n+1} = \bar{S}^{n+1} - \bar{S}_h^{n+1}$ . From (11) and (12), we have

$$\begin{aligned} \delta^{n+1} - \delta^n &= F(S^n) \Delta t - F(I(\bar{S}_h^n)) \Delta t + o(\Delta t) \\ &= [F(S^n) - F(I(\bar{S}^n))] \Delta t + [F(I(\bar{S}^n)) - F(I(\bar{S}_h^n))] \Delta t + o(\Delta t). \end{aligned}$$

In [1] we showed for the local approach that

$$\begin{aligned} |\delta^n| &\leq o(\Delta t) + \Delta t \sum_{k=0}^{n-1} (1 + C \Delta t)^k |F(S^{n-k}) - F(I(\bar{S}^{n-k}))| \\ &\leq o(\Delta t) + \left[ \frac{e^{C(n \Delta t)} - 1}{C} \right] \left[ \max_{1 \leq i \leq n} |F(S^i) - F(I(\bar{S}^i))| \right]. \end{aligned}$$

This result is valid in the regions away from sharp interfaces because the proof assumes that  $F(I(\bar{S}))$  is a smooth function of  $\bar{S}$  which does not hold, in general, in the regions of sharp interfaces.

In [1], an estimate for  $\delta^n$  is presented when the inlet boundary conditions for the saturation is chosen *a priori*. The typical inlet boundary conditions are  $S_{in} = 1$  at the inlet, as it was mentioned earlier, or the use of single-phase flow information based on time of flight function. The latter is motivated by an analysis which shows that  $S$  is a smooth function of time of flight. The analysis reveals two type of errors; (1) errors due to the variations of the saturation along the inlet boundaries (2) errors due to the evolution of the saturation along each streamline.

In the global approach, the saturation values at previous (coarse) time step is used to impose inlet boundary conditions for (9). This approach will therefore generally give more accurate solutions than the previously proposed local approach where *a priori* inlet boundary conditions are imposed for the saturation. However, because the saturation basis functions are sampled from the solution obtained with (10) where the inlet boundary conditions on the boundary of each coarse grid block are not changed during the time interval corresponding to a coarse time step, the proposed approach introduces errors. Moreover, if the velocity differs from the velocity

in the initial DDM simulation from which the saturation basis functions are sampled, e.g., if the permeability field has been perturbed as part of an history matching loop, then an additional error occurs. We discuss now briefly the nature and influence of these errors.

First, to understand the error due the fact that the DDM employs static inlet boundary conditions for the duration of each coarse time step, we consider the saturation equation on time of flight coordinates given by (assume for simplicity  $\phi = 1$ )

$$v \cdot \nabla \tau = 1.$$

Then, the saturation equation along each streamline becomes

$$\frac{\partial S}{\partial t} + \frac{\partial f(S)}{\partial \tau} = 0.$$

If the velocity variation over the coarse time interval  $[t, t + \Delta t]$  is small, then the error due to unchanged value of the saturation at the inlet boundary can be estimated by maximum change of  $|S(\tau, t + \Delta t) - S(\tau, t)|$ . Because this term reflects the saturation change in  $[t, t + \Delta t]$  (which is  $\Delta t \int_{\partial T} f(S)(v \cdot n) ds$ ) it is  $o(\Delta t)$ . Thus, imposing the saturation value at previous coarse time step, introduces an error of order  $o(\Delta t)$  along each streamline. Consequently, the variation of the saturation along the inlet is of order  $o(\Delta t)$  and it is consistent with the reference fine-scale saturation distribution at the inlet. From here, we obtain that the saturation error at the inlet boundaries is small, and consequently,  $\delta^n$  is small.

Next, we discuss the error due to velocity change. In the proposed approach, the velocity change occurs due to mobility (total permeability) changes in multi-phase flows. These changes will generally not alter flow patterns (streamlines) substantially. Permeability changes that do not significantly alter streamlines also occur during certain history matching approaches. If the permeability is modified so that the large scale flow patterns resemble closely the flow patterns in the initial DDM simulation, then the corresponding multiscale basis functions for the saturation can be applied. The reason why the streamlines are not significantly changed is that flow patterns are often dominated by source and sink (well) configurations, and that a simple scaling of the permeability does not alter the streamlines, it only rescales the velocity along the streamlines. Hence, when the source and sink configuration is not changed, and the permeability field is perturbed in a way that retains the dominating large scale heterogeneity structures, then the fine-scale velocity field will basically be re-scaled by a coarse-scale time dependent function. Because the interpolation operators are invariant with respect to re-scaling of the velocity field (cf. [1]), the saturation solution error caused by a small perturbation of the velocity field will be small in general. This observation is supported by the numerical results in the next section.

The errors due to small perturbations of streamlines can be analyzed by introducing an additional time of flight function for perturbed streamlines and estimating the difference between the saturation fields via the difference of time of flights. We have performed similar analysis in [2] for estimating the error due to adaptive coarsening and omit this discussion here.

The above argument does not hold for the regions of sharp interfaces. If a sharp interface passes through several coarse blocks during  $[t, t + \Delta t]$ , then the  $L_\infty$  error in the saturation will be of order  $O(1)$  due to the error in the location of sharp interface. The error will result in a saturation error in  $L_1$  norm of order of coarse mesh size. Sharp interfaces may, however, be tracked separately using an adaptivity criteria [1].

## 5. NUMERICAL RESULTS

In the current section we test the proposed methodology on a synthetic reservoir with corner-point grid geometry. The corner-point grid has vertical pillars, as shown in Figure 1, 100 layers,

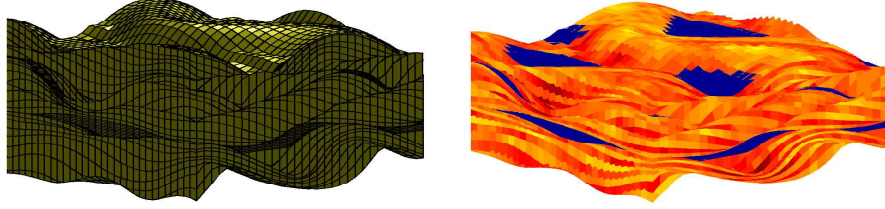


FIGURE 1. A corner-point model with vertical pillars and 100 layers. To the right is a plot of the permeability field on a logarithmic scale. The model is generated with SBED<sup>TM</sup>, and is courtesy of Alf B. Rustad at STATOIL.

and 29629 active cells (cells with positive volume). The permeability ranges from 0.1 mD to 1.7 D, the porosity is assumed to be constant, and the water and oil mobilities are defined by

$$\lambda_w(S) = \frac{S^2}{\mu_w} \quad \text{and} \quad \lambda_o(S) = \frac{(1-S)^2}{\mu_o}, \quad (13)$$

where we assume that the oil and water viscosities are equal:  $\mu_w = \mu_o = 0.003$  cp.

The coarse grid (for both the MsMFEM and the multiscale method for transport) is constructed by subdividing the corner-point grid, consisting of 30-by-30-by-100 corner point cells, into 6-by-6-by-20 grid blocks with equal number of corner-point cells. Note however that the grid blocks do not contain the same number of active cells. Indeed, some grid blocks are non-active so that the total number of grid blocks is 538. Hence, although the corner-point grid is logically Cartesian, it is unstructured in physical space. However, unlike fully unstructured grids, the logical Cartesian format allows us to coarsen the grid “uniformly” in the logical index space. The use of different coarsening strategies has been explored for the MsMFEM in [4].

The corner-point grid serves as the subgrid for the multiscale method for transport. The basis functions for the MsMFEM are computed using the lowest-order Raviart-Thomas mixed FEM on a conforming tetrahedral subgrid of the corner-point grid. The tetrahedral grid contains 147344 non-degenerated tetrahedrons. We want to emphasize that although the MsMFEM basis functions are recomputed only if flow conditions change, the pressure equation (1) is solved repeatedly to account for mobility variations.

To measure the overall accuracy of a saturation solution we compute the error in the fine- and coarse-grid saturation profiles relative to a reference solution,

$$e(S, S_{\text{ref}}, t) = \frac{\|\phi S_{\text{ref}}(\cdot, t) - \phi S(\cdot, t)\|_{L^2}}{\|\phi S_{\text{ref}}(\cdot, t) - \phi S_{\text{ref}}(\cdot, 0)\|_{L^2}}.$$

Here time is measured in pore-volumes injected (PVI), i.e., time measures the fraction of the total accessible pore-volume in  $\Omega$  that has been injected into  $\Omega$ . The reference solution  $S_{\text{ref}}$  is computed using an implicit upstream method on the corner-point grid. Moreover, to see if the multiscale method resolves high flow regions adequately, we compare water-cut curves (fraction of water in the produced fluid) for the solution  $S_{\text{Ms}}$  obtained using the multiscale method with water-cut curves corresponding to the reference solution, and a coarse-grid solution  $S_C$  obtained by solving the saturation equation on the coarse grid with an implicit upstream method.

We consider first a test-case where we inject water at a fixed rate along a vertical column at one of the corners, and produce at a fixed rate along a vertical column at the opposite corner. For this problem we consider only the local approach to generating saturation basis functions. Figure 2 shows the respective water-cut curves, and how the saturation error evolves during the simulation for  $S_{\text{Ms}}$  and  $S_C$ . The results illustrate that the multiscale method with basis functions generated using the local approach gives a moderate improvement over the coarse grid

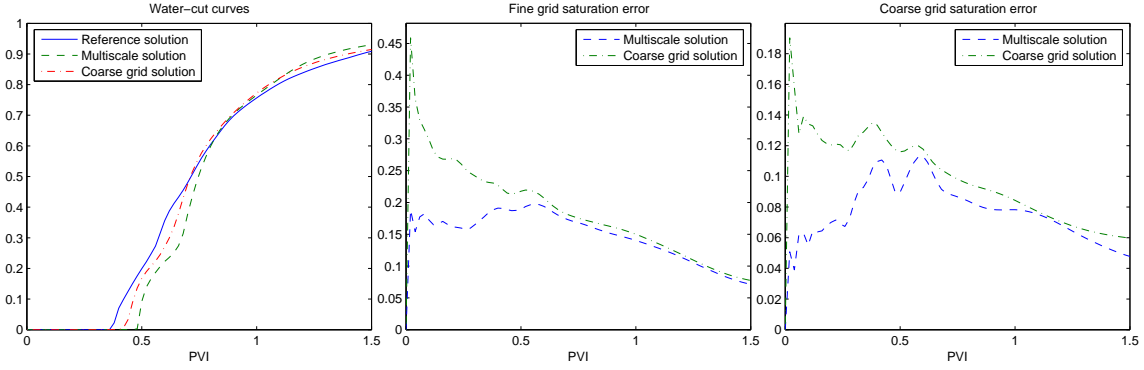


FIGURE 2. Left: water-cut curves for  $S_{\text{ref}}$ ,  $S_{\text{Ms}}$ , and  $S_C$ . Middle:  $e(S_{\text{Ms}}, S_{\text{ref}}, t)$  and  $e(S_C, S_{\text{ref}}, t)$ . Right:  $e(\bar{S}_{\text{Ms}}, \bar{S}_{\text{ref}}, t)$  and  $e(\bar{S}_C, \bar{S}_{\text{ref}}, t)$ .

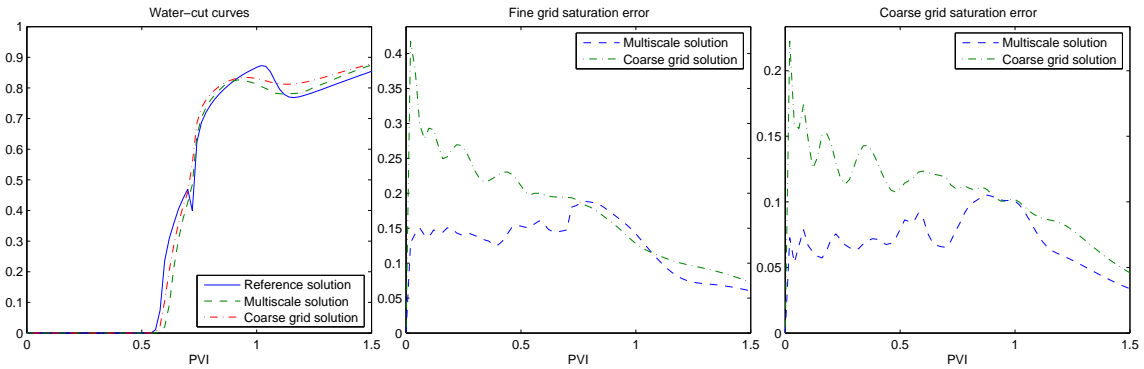


FIGURE 3. Water-cut curves and fine and coarse grid saturation errors for the case with perturbed permeability field, and changed flow conditions at 0.7 PVI.

solution in terms of overall accuracy of the saturation profiles. Both solutions produce water-cut curves that match reasonably well the water-cut curve produced by the reference solution.

Next, we apply the multiscale method with basis functions generated using the global approach on the original model to run a simulation with a perturbed permeability field. The perturbation is performed by multiplying the permeability in each grid cell  $K_i$  cell by  $10^{\delta_i}$ , where  $\delta_i$  is a random value in the interval  $(-2, 2)$ . The perturbed permeability ranges roughly from  $10^{-6}$  to  $10^2$  D. The well locations are changed at 0.7 PVI. That is, if, say, corner 4 is opposite to corner 1, and corner 3 is opposite to corner 2, then we inject at corner 1 and produce at corner 4 for  $t < 0.7$  PVI. For  $t > 0.7$  PVI we inject at corner 2 and produce at corner 3. The results in Figure 3 demonstrate that, although perturbing the data changes the fine-grid saturation solution locally, the multiscale method continues to give better accuracy than the coarse scale solution on both coarse and fine grids, and to provide relatively accurate water-cut curves.

Finally we perform a simulation with the same set-up as above, but now with a high mobility ratio, i.e., with  $\mu_o = 10\mu_w$ . Figure 4 shows that the results obtained for this case are qualitatively similar to the results in Figure 3 that were obtained with  $\mu_o = \mu_w$ . In addition, in Figure 5 we plot the three saturation solutions (reference, multiscale, and coarse grid) at 0.5 PVI, 1 PVI, and 1.5 PVI. Notice the effect of altered well-locations in Figure 4 (b) relative to Figure 4 (a).

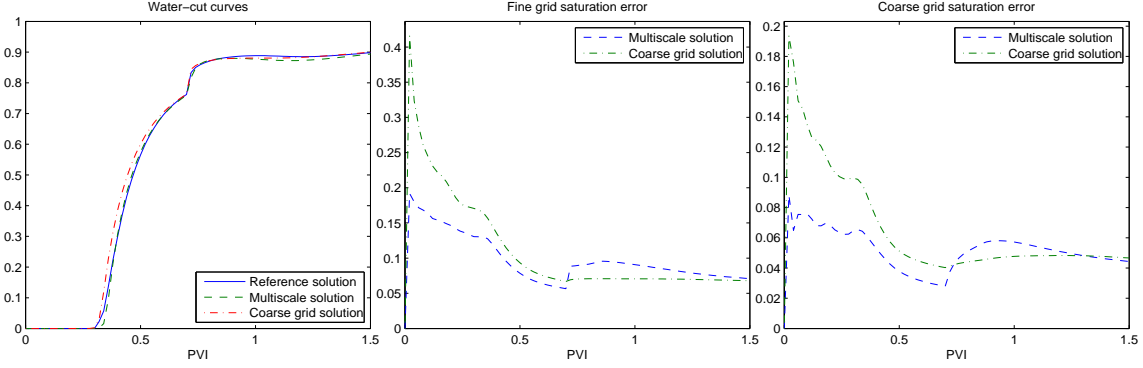


FIGURE 4. Water-cut curves and fine and coarse grid saturation errors for case with  $\mu_o = 10\mu_w$ , perturbed permeability field, and changed flow conditions at 0.7 PVI.

## 6. CONCLUDING REMARKS

The main purpose of this paper has been to introduce a multiscale method for solving transport equations that arise in models for immiscible two-phase flow in porous media. The basic idea is to use information from a velocity field with subgrid resolution that is obtained using a multiscale mixed finite element method to improve accuracy of flow simulations on coarse grids. The algorithm proceeds in two steps: first the flow is computed on a coarse grid, and then the coarse grid solution is projected onto a finer subgrid. The subgrid solution is used in the coarse grid equations, along with fine grid velocities, to enhance the accuracy of the coarse grid solution. Thus, the construction of pseudo relative permeability functions are avoided, and fine scale structures in the velocity field are treated in a mathematically consistent manner. The methodology has been applied to immiscible and incompressible two-phase flow on a synthetic reservoir model with corner-point grid geometry. The numerical results demonstrate that the multiscale method for the transport provides more accurate solutions than a standard coarse grid solution, and can serve as a more robust alternative to two-phase flow upscaling.

## REFERENCES

1. J. E. Aarnes and Y. Efendiev, *An adaptive multiscale method for simulation of fluid flow in heterogeneous porous media*, Multiscale Model. Simul. **5** (2006), no. 3, 918–939.
2. J. E. Aarnes, V. L. Hauge, and Y. Efendiev, *Coarsening of three-dimensional structured and unstructured grids for subsurface flow*, Submitted to Adv. Water Res. (2006).
3. J. E. Aarnes, S. Krogstad, and K.-A. Lie, *A hierarchical multiscale method for two-phase flow based upon mixed finite elements and nonuniform coarse grids*, Multiscale Model. Simul. **5** (2006), no. 2, 337–363.
4. ———, *Multiscale mixed/mimetic methods on corner-point grids*, Comput. Geosci. (to appear).
5. J.E. Aarnes, *On the use of a mixed multiscale finite element method for greater flexibility and increased speed or improved accuracy in reservoir simulation*, Multiscale Model. Simul. **2** (2004), no. 3, 421–439.
6. T. Arbogast, *Analysis of a two-scale, locally conservative subgrid upscaling for elliptic problems*, Siam J. Numer. Anal. **42** (2004), 576–598.
7. I. Babuška and E. Osborn, *Generalized finite element methods: Their performance and their relation to mixed methods*, SIAM J. Numer. Anal. **20** (1983), 510–536.
8. J.W. Barker and S. Thibeau, *A critical review of the use of pseudorelative permeabilities for upscaling*, SPE Reservoir Eng. (1997), no. 12, 138–143.
9. Z. Chen and T.Y. Hou, *A mixed multiscale finite element method for elliptic problems with oscillating coefficients*, Math. Comp. **72** (2003), 541–576.
10. M.A. Christie, *Upscaling for reservoir simulation*, JPT J. Pet. Tech. (1996), no. 48, 1004–1010.

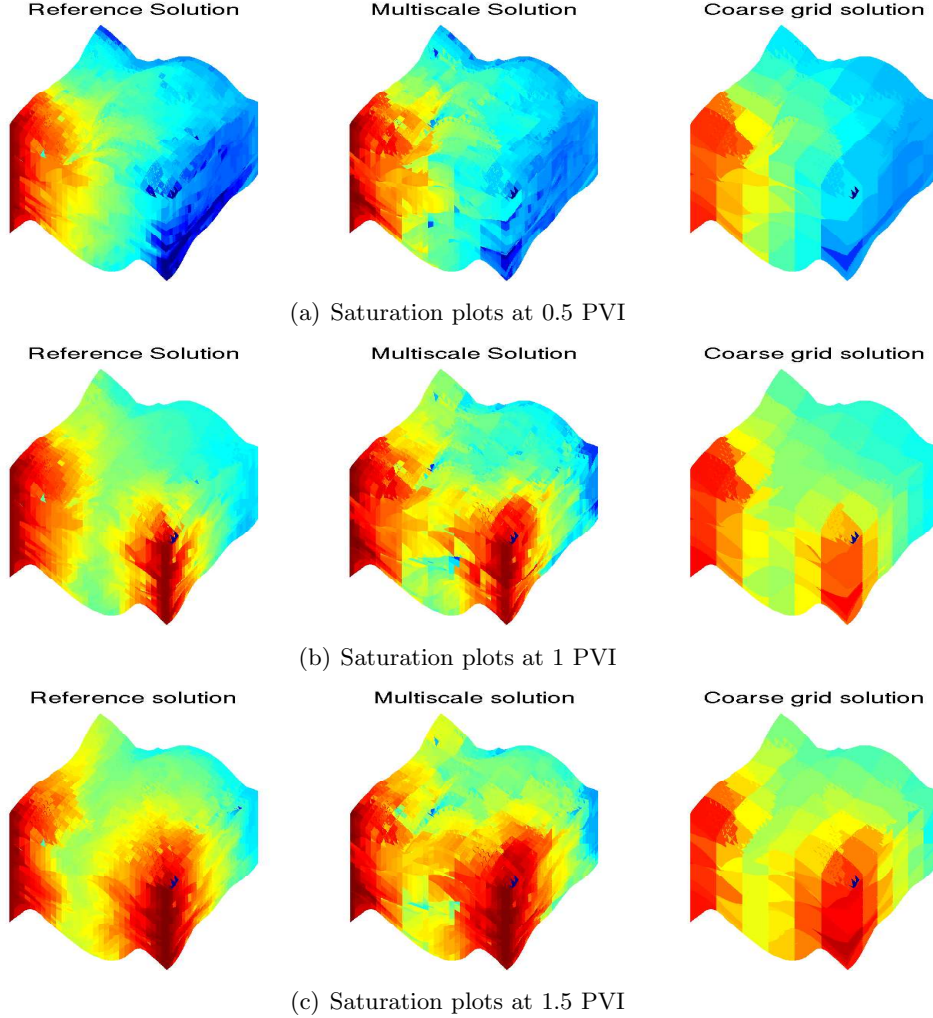


FIGURE 5. Saturation plots at 0.5 PVI, 1 PVI, and 1.5 PVI for case with  $\mu_o = 10\mu_w$ , perturbed permeability field, and changed flow conditions at 0.7 PVI.

11. Y. Efendiev, V. Ginting, T. Y. Hou, and R. Ewing, *Accurate multiscale finite element methods for two-phase flow simulations*, J. Comput. Phys., to appear.
12. Y. Efendiev, T. Hou, and V. Ginting, *Multiscale finite element methods for nonlinear problems and their applications*, Commun. Math. Sci. **2** (2004), no. 4, 553–589.
13. T.Y. Hou and X-H. Wu, *A multiscale finite element method for elliptic problems in composite materials and porous media*, J. Comput. Phys. **134** (1997), 169–189.
14. P. Jenny, S. H. Lee, and H. A. Tchelepi, *Multi-scale finite-volume method for elliptic problems in subsurface flow simulation*, J. Comput. Phys. **187** (2003), 47–67.
15. J.R. Kyte and D.W. Berry, *New pseudofunctions to control numerical dispersion*, SPE (1975), no. 5105.
16. H.L. Stone, *Rigorous black-oil pseudofunctions*, SPE (1991), no. 21207.